ELSEVIER

Catalysis Today 64 (2001) 253–269

CATALYSIS TODAY

www.elsevier.com/locate/cattod

Hydrodynamics of churn turbulent bubble columns: gas–liquid recirculation and mechanistic modeling

Puneet Gupta [a], Booncheng Ong [a], Muthanna H. Al-Dahhan [a,*], Milorad P. Dudukovic [a], Bernard A. Toseland [b]

[a] *Department of Chemical Engineering, Chemical Reaction Engineering Laboratory (CREL), Campus Box 1198, 1 Brookings Drive, Washington University, St. Louis, MO 63130-4899, USA*

[b] *Air Products and Chemicals, Inc., PO Box 25780, Lehigh Valley, PA 18007, USA*

Abstract

A phenomenological (mechanistic) model has been developed for describing the gas and liquid/slurry phase mixing in churn turbulent bubble columns. The gas and liquid phase recirculation rates in the reactor, which are needed as inputs to the mechanistic reactor model are estimated via a sub-model which uses the two-fluid approach in solving the Navier–Stokes equations. This sub-model estimates the effective bubble diameter in the reactor cross-section and provides a consistent basis for the estimation of the volumetric mass transfer coefficients. The strategy for the numerical solution of the sub-model equations is presented along with the simulation results for a few cases. The overall reactor model has been tested against experimental data from radioactive gas tracer experiments conducted at the Alternate Fuels Development Unit (AFDU), La Porte, TX under conditions of methanol synthesis. © 2001 Elsevier Science B.V. All rights reserved.

Keywords: Gas–liquid flow; Slurry bubble column; Computed tomography; Radioactive particle tracking; Gas–liquid recirculation; Mechanistic reactor modeling; Radioactive tracer studies

1. Introduction

The abundance of natural gas in many remote areas has led to a continued interest in natural gas conversion to liquid fuels and chemicals that can be easily and economically transported. Such conversion of natural gas to value-added liquid products is generally accomplished in two-stages. In the first stage, natural gas is transformed to a mixture of hydrogen and carbon monoxide (synthesis gas), which in the second stage can be converted to a whole range of valuable chemicals depending on the catalyst and the employed process conditions. Liquid phase methanol synthesis, synthesis of Fischer–Tropsch (FT) liquids and a host of other processes based on syngas chemistries have been reported [1]. Traditionally, these processes were realized using fixed bed reactors, however, recently slurry bubble column reactors have become the reactors of choice. This change occurred owing to the excellent heat and mass transfer characteristics of slurry bubble column reactors and because this reactor type offers the possibility of greatly increased production capacities resulting from increased gas throughputs [2].

Conventional bubble column reactors have been in use for decades in many chemical processes, and consequently, a vast body of literature on bubble column

* Corresponding author. Tel.: +1-314-935-7187; fax: +1-314-935-7211.
E-mail address: muthanna@wuche.che.wustl.edu (M.H. Al-Dahhan).

0920-5861/01/$ – see front matter © 2001 Elsevier Science B.V. All rights reserved.
PII: S0920-5861(00)00529-0

Nomenclature

a	interfacial area (cm^{-1})
B	number of bubbles formed per unit volume per unit time ($cm^{-3}\,s^{-1}$)
C	concentration (mol/cm^3)
C_D	drag coefficient
C_{vm}	virtual mass coefficient
c	parameter in the holdup profile to allow non-zero holdup at the wall
D_C	column diameter (cm)
$D_{L,m}$	molecular diffusivity (cm^2/s)
$\bar{D}_{rr}$	radial turbulent diffusivity (cm^2/s)
$\bar{D}_{xx_1}$	axial turbulent diffusivity of small bubbles and liquid going up (cm^2/s)
$\bar{D}_{xx_2}$	axial turbulent diffusivity of small bubbles and liquid going down (cm^2/s)
d_b	mean bubble diameter (cm)
Eo	Eotvos number
g	acceleration due to gravity (cm^2/s)
H	Henry's constant
k	mass transfer coefficient (cm/s)
L	dispersion height between the two CSTRs (cm)
l	mixing length (cm)
m	power law exponent in the radial gas holdup profile
P	operating pressure (dyn/cm^2)
Q	flow rate (cm^3/s)
R	column radius (cm)
R_x	reaction rate ($mol\,cm^{-3}\,s^{-1}$)
r	radial position in the column (cm)
r'	radius where the liquid velocity profile inverts
r''	radius where the gas velocity profile inverts
t	time (s)
$U_{G,sup}$	gas superficial velocity (cm/s)
$U_{L,sup}$	liquid superficial velocity (cm/s)
u	velocity (cm/s)
$\bar{u}$	radially averaged mean velocity (cm/s)
V_a	volume of the CSTR representing the distributor zone (cm^3)
V_b	volume of the CSTR representing the disengagement zone (cm^3)
x	axial position in the column (cm)

Greek symbols

ε	local phase holdup
$\bar{\varepsilon}$	radially averaged phase holdup
$\tilde{\varepsilon}_g$	parameter in the gas holdup profile related to $\bar{\varepsilon}_g$
$\bar{\varepsilon}'_{g1}$	mean holdup of up-flowing gas with down-flowing liquid
μ_l^m	liquid/slurry viscosity (cP)
ν^m	kinematic viscosity (cm^2/s)
ν^t	turbulent viscosity (cm^2/s)
ξ	dimensionless radius
ξ'	dimensionless radius where the liquid velocity profile inverts
ξ''	dimensionless radius where the gas velocity profile inverts
ρ	density (g/cm^3)
σ	surface tension of the liquid (dyn/cm)
τ^m	viscous shear stress (dyn/cm^2)
τ^t	turbulent shear stress (dyn/cm^2)
ϕ	fraction of the column diameter

Subscripts

CST	well mixed distributor and disengagement zones, a and b
g	gas
ga	gas phase in the distributor zone, CST a
gb	gas phase in the disengagement zone, CST b
gdld	gas going down with liquid down as well
guld	gas flowing upwards with liquid going down
gulu	gas flowing upwards with liquid going up as well
g1	up-flowing gas
g2	down-flowing gas
in	reactor inlet
l	liquid
la	liquid phase in the distributor zone, CST a
lb	liquid phase in the disengagement zone, CST b
l1	up-flowing liquid
l2	down-flowing liquid
out	reactor outlet

reactors has grown since the 1950s [3–8]. Until the late 1980s, only the average hydrodynamic properties of these reactors, viz., overall gas holdup, overall volumetric mass transfer coefficients, overall gas and liquid phase dispersion, were reported. However, with the advent of modern computing capabilities and advances in the sophisticated measurement techniques, characterization of the local hydrodynamics, both experimentally and numerically, has become possible during the last decade [9–18].

To predict reactor performance based on detailed hydrodynamic and mixing phenomena occurring in large-scale bubble column flows, mathematical modeling and numerical simulation using the two-fluid model has been frequently practiced. However, the choice of the correct closures and phase interaction terms needed to give accurate predictions of flow patterns by computational fluid dynamics (CFD) simulations is still a matter of art. This arises because the phenomena governing the multiphase hydrodynamics occur on many scales. However, measurement at many scales under actual operating conditions is still in its infancy with the common measurement techniques being limited to the characterization of the global and large-scale properties only. Therefore, it is the modeling of the small-scale phenomena and their coupled interactions with those at larger scales that limits the capability of CFD in serving as a stand-alone tool for prediction of bubble column reactor performance.

Given this state-of-the-art, it is quite likely that reliable predictions of reactor performance using multiphase CFD are a decade or more away. Therefore, for efficient design of slurry bubble column reactors, it is desirable to have models that are able to capture the majority of the physical phenomena and provide a reasonably reliable and fundamentally based method for design and scale-up. This goal is especially important for reactors involving complex chemistries in industrially relevant very large-scale systems such as FT. The most commonly used model of this type, the axial dispersion model (ADM), has had only limited success in retrofitting experimental data. Mechanistic modeling offers the possibility of incorporating the relevant observable physics in describing liquid phase mixing [19–21] and offers a path to efficient design. We have used this approach to develop a mechanistic model that incorporates modeling the flow of not only the liquid but also of the gas phase.

Here, we present only a brief summary of the reactor model and focus on the development of a sub-model for predicting the long-time averaged gas and liquid recirculation velocities, which form the basis for the developed reactor model. Our approach is based on the Euler–Euler two-fluid representation of the momentum balance equations for the gas and liquid phases [11]. A number of investigators [22–26] have reported a similar model to describe liquid recirculation. However, we modify the model equations and closures used for the liquid phase turbulence. In particular, the momentum balance equations have been derived from the two-fluid equations, and the recirculation model has been extended to calculate the radial profile of the axial gas phase velocity.

2. Phenomenological reactor model

The observed hydrodynamic phenomena in a typical bubble column operation are represented schematically in Fig. 1 and form the basis of the mechanistic reactor model. In the time average sense, the radial

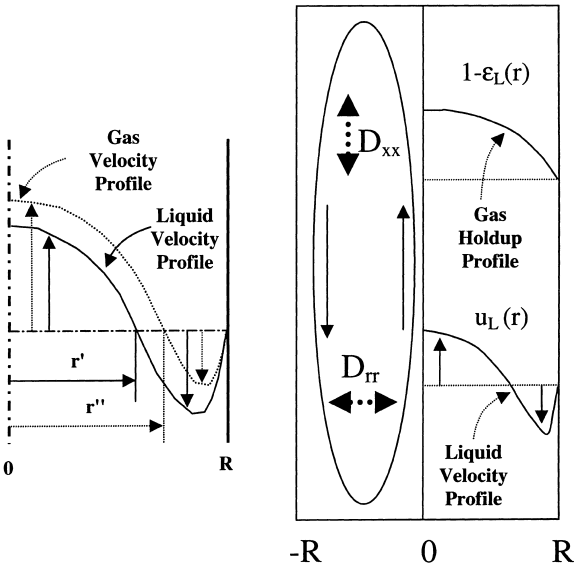

Fig. 1. Schematic representation of the experimentally observed phenomena in bubble columns.

gas holdup distribution results in a single liquid recirculation loop with the liquid rising in the center and flowing downwards near the walls [21]. Most of the gas travels upwards through the column center and leaves the reactor above the liquid-free surface at the top. However, some small-sized bubbles do not possess enough momentum to disengage and leave the reactor and recirculate along with the liquid. In addition to this convective recirculation, momentum transport is caused by the bubble wakes, bubble–bubble interactions and shear-induced turbulence — typically called 'eddy diffusion'. This physical picture is the result of numerous experimental studies on liquid recirculation reported in the literature [27–31], and of the extensive studies conducted by the non-invasive measurement techniques at the Chemical Reaction Engineering Laboratory (CREL) in Washington University, St. Louis, MO consisting of computed tomography (CT) and computer automated radioactive particle tracking (CARPT) [21,32–36]. CT provides non-invasive measurement of the long-time averaged, cross-sectional distribution of the gas holdup in any reactor cross-section. The details of the γ-ray scanner and associated tomography reconstruction algorithms developed in CREL have been discussed elsewhere [34,35]. CARPT on the other hand provides information on the long-time averaged liquid velocity profile, turbulent stresses and eddy diffusivities. Details of the principles and methodology of the CARPT technique have also been discussed elsewhere [21,32,33].

The compartmentalization of the mechanistic (phenomenological) model is shown in Fig. 2, and this represents a modification and extension of the model proposed by Wang [37]. The net flow of liquid could be either zero (batch mode of operation) or a co-current up-flow with the net flow of the gas. In either case, the liquid flow pattern inside the reactor consists of up-flow (L_1) in the core and down-flow (L_2) near the wall. The gas phase also has a similar recirculation pattern; with up-flow in the center (G_1), and down flow by the wall (G_2) consisting of bubbles which do not possess sufficient momentum and get recirculated along with the liquid. The upward flowing gas usually consists of relatively small bubbles trapped in the wakes of the larger fast rising bubbles, and drags the liquid along with it. The top (disengagement) and the bottom (distributor) zones

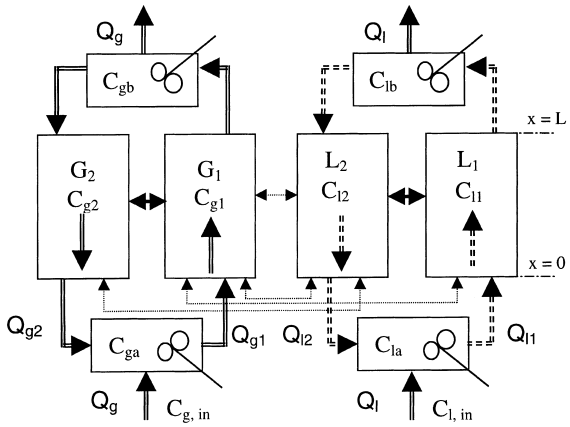

Fig. 2. Schematic representation of the compartmentalization of the reactor.

are modeled as being well mixed (continuous stirred tanks (CSTs)) and their height is taken to be the same as the column diameter D_C. Changing the height of these zones between $0.5D_C$ and $2.0D_C$ does not have a noticeable effect on the extent of liquid backmixing [20], provided the height of the gas–liquid mixture is much larger than the column diameter (L/D_C is at least 6). It has been found [38] that the effect of the height of these zones on the gas phase tracer responses is insignificant as well.

A differential element along the reactor length in the developed part of the flow, which occupies most of the column, consists of four zones into which the reactor cross-section is compartmentalized. By applying mass balances for a soluble species to each of these zones within the differential element, one obtains four transient convection–diffusion partial differential equations (PDEs) with mass interphase transfer and radial exchange between the zones acting as source terms. Additional source terms appear in the form of reaction rates, if simulations are being carried out for a reactive species in a bubble column reactor operated under reaction conditions. On the other hand, the equations describing the dynamics of the perfectly mixed tanks representing the distributor and disengagement zones are only ordinary differential equations (ODEs). Therefore, the reactor model results in a coupled set of four PDEs and four ODEs as summarized below for a representative chemical species.

For the gas moving upwards (G_1):

$$\frac{\partial C_{g1}}{\partial t} = \bar{D}_{xx_1}\frac{\partial^2 C_{g1}}{\partial x^2} - \bar{u}_{g1}\frac{\partial C_{g1}}{\partial x} - \frac{4(\bar{D}_{rr}\varepsilon_g)_{r=r''}}{r''R\bar{\varepsilon}_{g1}}(C_{g1} - C_{g2}) + R_{x,g1} - \frac{k_{gulu}a_{gulu}}{\bar{\varepsilon}_{g1}}(HC_{g1} - C_{l1}) - \frac{k_{guld}a_{guld}}{\bar{\varepsilon}_{g1}}(HC_{g1} - C_{l2}) \quad (1)$$

For the gas moving downwards (G_2):

$$\frac{\partial C_{g2}}{\partial t} = \bar{D}_{xx_2}\frac{\partial^2 C_{g2}}{\partial x^2} + \bar{u}_{g2}\frac{\partial C_{g2}}{\partial x} - \frac{k_{gdld}a_{gdld}}{\bar{\varepsilon}_{g2}} \times (HC_{g2} - C_{l2}) + \frac{4r''/R}{R^2 - r''^2}\frac{(\bar{D}_{rr}\varepsilon_g)_{r=r''}}{\bar{\varepsilon}_{g2}} \times (C_{g1} - C_{g2}) + R_{x,g2} \quad (2)$$

For the liquid moving upwards (L_1):

$$\frac{\partial C_{l1}}{\partial t} = \bar{D}_{xx_1}\frac{\partial^2 C_{l1}}{\partial x^2} - \bar{u}_{l1}\frac{\partial C_{l1}}{\partial x} + \left(\frac{r''}{r'}\right)^2 \frac{k_{gulu}a_{gulu}}{\bar{\varepsilon}_{l1}}(HC_{g1} - C_{l1}) - \frac{4(\bar{D}_{rr}\varepsilon_l)_{r=r'}}{r'R\bar{\varepsilon}_{l1}}(C_{l1} - C_{l2}) + R_{x,l1} \quad (3)$$

For the liquid moving downwards (L_2):

$$\frac{\partial C_{l2}}{\partial t} = \bar{D}_{xx_2}\frac{\partial^2 C_{l2}}{\partial x^2} + \bar{u}_{l2}\frac{\partial C_{l2}}{\partial x} + \frac{4r'/R}{R^2 - r'^2} \times \frac{(\bar{D}_{rr}\varepsilon_l)_{r=r'}}{\bar{\varepsilon}_{l2}}(C_{l1} - C_{l2}) + R_{x,l2} + \left(\frac{r''^2}{R^2 - r'^2}\right)\frac{k_{guld}a_{guld}}{\bar{\varepsilon}_{l2}}(HC_{g1} - C_{l2}) + \left(\frac{R^2 - r''^2}{R^2 - r'^2}\right)\frac{k_{gdld}a_{gdld}}{\bar{\varepsilon}_{l2}}(HC_{g2} - C_{l2}) \quad (4)$$

Gas in the distributor zone:

$$\frac{dC_{ga}}{dt} = \frac{\bar{\varepsilon}_{g2}\bar{u}_{g2}}{\bar{\varepsilon}_g\phi_{in}D_C}\frac{(R^2 - r''^2)}{R^2}C_{g2,0} - \frac{\bar{\varepsilon}_{g1}\bar{u}_{g1}}{\bar{\varepsilon}_g\phi_{in}D_C}\frac{r''^2}{R^2}C_{ga} + \frac{U_{G,sup}}{\bar{\varepsilon}_g\phi_{in}D_C}C_{g,in} - \frac{k_{CST}a_{CST}}{\bar{\varepsilon}_g}(HC_{ga} - C_{la}) + R_{x,ga} \quad (5)$$

Liquid in the distributor zone:

$$\frac{dC_{la}}{dt} = \frac{\bar{\varepsilon}_{l2}\bar{u}_{l2}}{\bar{\varepsilon}_l\phi_{in}D_C}\frac{(R^2 - r'^2)}{R^2}C_{l2,0} - \frac{\bar{\varepsilon}_{l1}\bar{u}_{l1}}{\bar{\varepsilon}_l\phi_{in}D_C}\frac{r'^2}{R^2}C_{la} + \frac{U_{L,sup}}{\bar{\varepsilon}_l\phi_{in}D_C}C_{l,in} + \frac{k_{CST}a_{CST}}{\bar{\varepsilon}_l}(HC_{ga} - C_{la}) + R_{x,la} \quad (6)$$

Gas in the disengagement zone:

$$\frac{dC_{gb}}{dt} = \frac{\bar{\varepsilon}_{g1}\bar{u}_{g1}}{\bar{\varepsilon}_g\phi_{out}D_C}\frac{r''^2}{R^2}C_{g1,L} - \frac{\bar{\varepsilon}_{g2}\bar{u}_{g2}}{\bar{\varepsilon}_g\phi_{out}D_C} \times \frac{(R^2 - r''^2)}{R^2}C_{gb} - \frac{U_{G,sup}}{\bar{\varepsilon}_g\phi_{out}D_C}C_{gb} - \frac{k_{CST}a_{CST}}{\bar{\varepsilon}_g}(HC_{gb} - C_{lb}) + R_{x,gb} \quad (7)$$

Liquid in the disengagement zone:

$$\frac{dC_{lb}}{dt} = \frac{\bar{\varepsilon}_{l1}\bar{u}_{l1}}{\bar{\varepsilon}_l\phi_{out}D_C}\frac{r'^2}{R^2}C_{l1,L} - \frac{\bar{\varepsilon}_{l2}\bar{u}_{l2}}{\bar{\varepsilon}_l\phi_{out}D_C}\frac{(R^2 - r'^2)}{R^2}C_{lb} - \frac{U_{L,sup}}{\bar{\varepsilon}_l\phi_{out}D_C}C_{lb} + \frac{k_{CST}a_{CST}}{\bar{\varepsilon}_l}(HC_{gb} - C_{lb}) + R_{x,lb} \quad (8)$$

2.1. Initial conditions

The initial conditions in all zones of the reactor are those of zero initial concentration of the species to be introduced at time $t = 0^+$ at the reactor inlet.

$$t = 0, \quad C_{la} = C_{lb} = C_{ga} = C_{gb} = C_{l1} = C_{l2} = C_{g1} = C_{g2} = 0 \quad (9)$$

The inlet function for describing the introduction of a species at the reactor inlet depends on the simulation objectives. For simulating the distribution evolution of a reactant species under reaction conditions, one would typically have a step change in the concentration of the species at the reactor inlet. However, here we are interested in simulating the distribution of a non-reacting tracer. Additionally, this initial condition for the tracer at the inlet depends on the method of tracer injection, and whether it is an impulse tracer test, or a step-up/step-down tracer test. For the results presented in this study, the experimental impulse input for the tracer runs at Alternate Fuels Development

Unit (AFDU), La Porte, TX has been simulated using a Gaussian function with a tail [21].

$$t \to 0^+, \quad t > 0, \quad C_{\mathrm{g,in}} = \frac{\psi}{\sqrt{2\pi\kappa t}} \exp\left\{-\frac{(\delta-\chi)^2}{2\kappa t}\right\}$$
$$C_{\mathrm{l,in}} = 0 \tag{10}$$

2.2. Boundary conditions for the fully developed region

Danckwerts boundary conditions are used at inlet and exit, guaranteeing preservation of mass for each phase. The bottom of the fully developed flow zone is the boundary with the CSTR representing the distributor zone, whereas the top of the fully developed flow zone is the boundary with the CSTR representing the disengagement zone. All the boundary conditions used are specified below.

Up-flow section of the gas:

$$x = 0, \quad \bar{u}_{\mathrm{g1}} C_{\mathrm{ga}} = \bar{u}_{\mathrm{g1}} C_{\mathrm{g1}}|_{x=0} - \bar{D}_{xx_1} \left.\frac{\partial C_{\mathrm{g1}}}{\partial x}\right|_{x=0} \tag{11}$$

$$x = L, \quad \left.\frac{\partial C_{\mathrm{g1}}}{\partial x}\right|_{x=L} = 0 \tag{12}$$

Down-flow section of the gas:

$$x = L, \quad \bar{u}_{\mathrm{g2}} C_{\mathrm{gb}} = \bar{u}_{\mathrm{g2}} C_{\mathrm{g2}}|_{x=L} + \bar{D}_{xx_2} \left.\frac{\partial C_{\mathrm{g2}}}{\partial x}\right|_{x=L} \tag{13}$$

$$x = 0, \quad \left.\frac{\partial C_{\mathrm{g2}}}{\partial x}\right|_{x=0} = 0 \tag{14}$$

Up-flow section of the liquid:

$$x = 0, \quad \bar{u}_{\mathrm{l1}} C_{\mathrm{la}} = \bar{u}_{\mathrm{l1}} C_{\mathrm{l1}}|_{x=0} - \bar{D}_{xx_1} \left.\frac{\partial C_{\mathrm{l1}}}{\partial x}\right|_{x=0} \tag{15}$$

$$x = L, \quad \left.\frac{\partial C_{\mathrm{l1}}}{\partial x}\right|_{x=L} = 0 \tag{16}$$

Down-flow section of the liquid:

$$x = L, \quad \bar{u}_{\mathrm{l2}} C_{\mathrm{lb}} = \bar{u}_{\mathrm{l2}} C_{\mathrm{l2}}|_{x=L} + \bar{D}_{xx_2} \left.\frac{\partial C_{\mathrm{l2}}}{\partial x}\right|_{x=L} \tag{17}$$

$$x = 0, \quad \left.\frac{\partial C_{\mathrm{l2}}}{\partial x}\right|_{x=0} = 0 \tag{18}$$

In the above set of equations, $\bar{D}_{xx}$ and $\bar{D}_{rr}$ are the average eddy diffusivities, which are estimated from a scale-up methodology developed by Degaleesan [21], based on the database established by CARPT. For description of other symbols used in the equations above, the reader is referred to the nomenclature. For the simulation results presented in this study for a non-reactive soluble gas tracer, the above model equations have been solved by a completely implicit finite difference scheme (FTCS — first order Forward differences in Time and second order Central differences in Space), which is robust and unconditionally stable. The treatment of the boundary conditions has been accomplished using ghost points. Since for simulation of tracer responses there are no non-linear terms in the equations, one needs to invert the matrix only once. This is accomplished by obtaining the LU decomposition of the matrix resulting from the application of the differencing scheme. The solution at successive times is simply obtained by matrix multiplication of the solution at previous time by repetitive LU back-substitution.

Before one can employ the numerical scheme discussed above for the solution of reactor model equations, one needs as inputs the hydrodynamic model parameters. As mentioned before, a sub-model for gas and liquid recirculation is needed for this purpose and is the outlined discussed below.

3. Two-fluid sub-model for gas and liquid phase axial momentum exchange

The starting point in the derivation of the one-dimensional model for the radial liquid and gas phase velocity profiles is the two-fluid model equations presented below. These equations are the result of the ensemble-averaged approach of Drew and Passman [11]. Here, the subscript 'l' denotes the continuous liquid/slurry phase, whereas the subscript 'g' denotes the dispersed gas phase, and both phases are considered incompressible.

Equations of continuity:

$$\text{Liquid/slurry}: \quad \frac{\partial \varepsilon_{\mathrm{l}}}{\partial t} + \nabla \cdot (\varepsilon_{\mathrm{l}} \boldsymbol{u}_{\mathrm{l}}) = 0 \tag{19}$$

$$\text{Gas}: \quad \frac{\partial \varepsilon_{\mathrm{g}}}{\partial t} + \nabla \cdot (\varepsilon_{\mathrm{g}} \boldsymbol{u}_{\mathrm{g}}) = 0 \tag{20}$$

Momentum equations:

$$\text{Liquid/slurry}: \quad \rho_l \varepsilon_l \left(\frac{\partial \boldsymbol{u}_l}{\partial t} + \boldsymbol{u}_l \cdot \nabla \boldsymbol{u}_l \right) = \rho_l \varepsilon_l \boldsymbol{g} - \varepsilon_l \nabla p - (\boldsymbol{M}_d + \boldsymbol{M}_{vm}) - \nabla \cdot (\varepsilon_l \tau_l) \quad (21)$$

$$\text{Gas}: \quad \rho_g \varepsilon_g \left(\frac{\partial \boldsymbol{u}_g}{\partial t} + \boldsymbol{u}_g \cdot \nabla \boldsymbol{u}_g \right) = \rho_g \varepsilon_g \boldsymbol{g} - \varepsilon_g \nabla p + (\boldsymbol{M}_d + \boldsymbol{M}_{vm}) - \nabla \cdot (\varepsilon_g \tau_g) \quad (22)$$

In the momentum balance equations, $\boldsymbol{M}_d$ is the drag force term, $\boldsymbol{M}_{vm}$ is the virtual mass term. The mathematical representation of these terms is shown in Eqs. (23)–(27).

$$\boldsymbol{M}_d = \frac{6 \varepsilon_l \varepsilon_g}{\pi d_b^3} \boldsymbol{F}_d \quad (23)$$

$$\boldsymbol{F}_d = \tfrac{1}{8} \rho_l \pi d_b^2 C_D |\boldsymbol{u}_l - \boldsymbol{u}_g| (\boldsymbol{u}_l - \boldsymbol{u}_g) \quad (24)$$

$$C_D = \max \left[\overbrace{\frac{24}{Re}(1 + 0.15\, Re^{0.687})}^{C_{D,2}}, \overbrace{\frac{8}{3} \frac{Eo}{Eo + 4}}^{C_{D,1}} \right] \quad (25)$$

$$\boldsymbol{M}_{vm} = \frac{1}{2} \varepsilon_l \varepsilon_g C_{vm} \left(\frac{D\boldsymbol{u}_l}{Dt} - \frac{D\boldsymbol{u}_g}{Dt} \right) \quad (26)$$

$$C_{vm} = 1 + 3.32 \varepsilon_g + O(\varepsilon_g^2) \quad (27)$$

where C_D is the drag coefficient for sufficiently contaminated systems [39], $Eo = g(\rho_l - \rho_g) d_b^2 / \sigma$ is the Eotvos number based on the bubble diameter and the liquid surface tension, and $Re = d_b |\boldsymbol{u}_l - \boldsymbol{u}_g| / \nu_l^m$ is the bubble Reynolds number.

In the well-developed flow region of the column, the flow in the time-averaged sense is axisymmetric with only the axial velocities being non-zero. Hence, the time-averaged liquid flow pattern is represented by a single radial profile of the axial velocity. These assumptions are well justified in view of the holdup profile database available at CREL via CT; the liquid velocity profile database via CARPT [21,32–36].

Under these assumptions, the equations of continuity for both the phases (Eqs. (19) and (20)) are identically satisfied and one cannot use the traditional approach of solving the Poisson equation for the pressure correction through the use of these continuity equations (as is done in 2D and 3D CFD codes). In addition, the left-hand side of the momentum equations for both the gas and liquid phase becomes zero, and so does the virtual mass term. Finally, due to no flow in the radial and azimuthal directions, the pressure is assumed to be independent of the radial and azimuthal coordinates, and the pressure gradient term in the momentum equations reduces to dp/dz.

After retaining the non-zero gradients and velocity components in the momentum equations for the two phases, one gets the following simplified equations:

$$\text{Liquid/slurry}: \quad 0 = -\rho_l \varepsilon_l g - \varepsilon_l \frac{dp}{dz} - M_d - \frac{1}{r} \frac{d}{dr} (r \varepsilon_l (\tau_{l,rz}^m + \tau_{l,rz}^t)) \quad (28)$$

$$\text{Gas}: \quad 0 = -\rho_g \varepsilon_g g - \varepsilon_g \frac{dp}{dz} + M_d - \frac{1}{r} \frac{d}{dr} (r \varepsilon_g (\tau_{g,rz}^m + \tau_{g,rz}^t)) \quad (29)$$

where

$$\tau_{l,rz}^m = -\mu_l^m \frac{du_l}{dr} \quad (30)$$

$$\tau_{g,rz}^m = -\mu_g^m \frac{du_g}{dr} \quad (31)$$

$$\tau_{l,rz}^t = \rho_l \overline{u'_{l,r} u'_{l,z}} \quad (32)$$

$$\tau_{g,rz}^t = \rho_g \overline{u'_{g,r} u'_{g,z}} \quad (33)$$

Since $\mu_g^m \approx O(10^{-1}) \mu_l^m$ and $\rho_g \approx O(10^{-1} - 10^{-2}) \rho_l$, one can neglect both the molecular as well as the turbulent shear stresses in the gas phase as compared to those in the liquid/slurry phase. Therefore, upon addition of Eqs. (28) and (29), one obtains

$$0 = -(\rho_g \varepsilon_g + \rho_l \varepsilon_l) g - \frac{dp}{dz} - \frac{1}{r} \frac{d}{dr} \left[r \varepsilon_l \left(\overbrace{\tau_{l,rz}^m + \tau_{l,rz}^t}^{\tau_{l,rz}} \right) \right] \quad (34)$$

In the above equation, the superscripts "m" and "t" refer to molecular (viscous) and turbulent contributions, and ε_g is the radial gas holdup profile, which is represented in terms of the following power law function

which fits well the available experimental data.

$$\varepsilon_g(\xi) = \bar{\varepsilon}_g \left(\frac{m+2}{m+2-2c} \right) (1 - c\xi^m) \tag{35}$$

where, $\xi = r/R$ is the non-dimensional radius and $\bar{\varepsilon}_g$ is the cross-sectional mean gas hold-up. Substituting for the radial gas holdup (Eq. (35)) in Eq. (34) and using $p' = -\mathrm{d}p/\mathrm{d}z/\rho_l g$, one gets, on integrating Eq. (34) with boundary condition $\tau_{l,rz} = 0$ at $\xi = 0$,

$$(1-\varepsilon_g)\tau_{l,rz} = \frac{\rho_l g R \xi}{2}(p' - 1) + \frac{(\rho_l - \rho_g) g R \bar{\varepsilon}_g \xi}{2} \frac{(m+2-2c\xi^m)}{(m+2-2c)} \tag{36}$$

After anticipating a downward maximum liquid velocity at dimensionless radius $\xi = \lambda$, one assigns $\tau_{l,rz}|_{\xi=\lambda} = 0$. Applying this condition to Eq. (36) eliminates p' and yields Eq. (37).

$$\tau_{l,rz}(\xi) = \frac{\rho_l (1-\gamma) g R c \bar{\varepsilon}_g \xi \lambda^m}{(m+2-2c)(1-\varepsilon_g(\xi))} \left(1 - \left(\frac{\xi}{\lambda} \right)^m \right) = \rho_l g R \beta(\xi) \tag{37}$$

where

$$\beta(\xi) = \frac{(1-\gamma) c \bar{\varepsilon}_g \xi \lambda^m}{(m+2-2c)(1-\varepsilon_g(\xi))} \left(1 - \left(\frac{\xi}{\lambda} \right)^m \right) \tag{38}$$

and $\gamma = \rho_g/\rho_l$. To obtain the liquid velocity profile from the above shear stress profile, a constitutive relationship (closure) is needed relating the turbulent shear stresses to the mean liquid velocity profile. The simplest closure in terms of turbulent kinematic viscosity is employed in Eq. (39).

$$\tau_{l,rz}(r) = -\rho_l (\nu_l^m + \nu_l^t) \frac{\mathrm{d}u_l}{\mathrm{d}r} = -\rho_l \nu_l^m \frac{\mathrm{d}u_l}{\mathrm{d}r} - \rho_l l^2 \left| \frac{\mathrm{d}u_l}{\mathrm{d}r} \right| \frac{\mathrm{d}u_l}{\mathrm{d}r} \tag{39}$$

The turbulent eddy viscosity ν_l^t can be closed by a modified mixing length $l(\xi)$ as given by Kumar et al. [22].

$$\nu_l^t = l^2 \left| \frac{\mathrm{d}u_l}{\mathrm{d}r} \right| \tag{40}$$

$$l(\xi) = \left\{ \frac{a(1-\xi)}{(\xi+b)^c} + d(1-\xi)^e \right\} R \tag{41}$$

The parameters a, b, c, d and e have been obtained by Kumar et al. [22] after considering extensive data on liquid recirculation velocities from CARPT, and results from experiments of other researchers who have made measurements of the liquid recirculation velocity by other experimental means. In this work, two other mixing length models are also used to assess the effect of this parameter on the simulation results. These are the mixing length profile of Nikuradse [40] and that of Joshi [41].

$$\text{Nikuradse}: \quad l(\xi) = \{0.14 - 0.08\xi^2 - 0.06\xi^4\} R \tag{42}$$

$$\text{Joshi}: \quad l(\xi) = 0.16R \tag{43}$$

Based on the above Eq. (39) becomes

$$\frac{\mathrm{d}u_l}{\mathrm{d}\xi} = \begin{cases} \dfrac{\nu_l^m R}{2l^2} \left(1 - \sqrt{1 + \dfrac{4l^2 g R}{\nu_l^{m^2}} \beta(\xi)} \right) & \text{for } 0 \le \xi \le \lambda \\ -\dfrac{gR^2}{\nu_l^m} \beta(\xi) & \text{for } \lambda \le \xi \le 1 \end{cases} \tag{44a,b}$$

3.1. Solution procedure

The boundary conditions to be used for the solution of the above equations are $u_l = 0$ at $\xi = 1$, and $\mathrm{d}u_l/\mathrm{d}\xi = 0$ at $\xi = 0$. Superimposed on this is the constraint that overall continuity for the liquid phase must be satisfied (note that the integral is split at $\xi = \lambda$ which is not the point of inversion of the liquid velocity profile, rather the point of maximum downward liquid velocity).

$$U_{L,\mathrm{sup}} = 2\int_{\xi=0}^{\xi=1} \{1 - \varepsilon_g(\xi)\} u_l(\xi) \xi \, \mathrm{d}\xi = 2\int_{\xi=0}^{\xi=\lambda} \{1 - \varepsilon_g(\xi)\} u_l(\xi) \xi \, \mathrm{d}\xi + 2\int_{\xi=\lambda}^{\xi=1} \{1 - \varepsilon_g(\xi)\} u_l(\xi) \xi \, \mathrm{d}\xi \tag{45}$$

It is this constraint, expressed by Eq. (45), that allows one to iterate on $\mathrm{d}p/\mathrm{d}z$ and obtain a converged solution. The numerical solution algorithm is as follows.

- Guess a value for λ (generally 0.9 is a good starting point).
- Calculate $u_{\mathrm{l},\lambda}$ by integrating Eq. (44a) from the boundary at $\xi = 1$ to $\xi = \lambda$:

$$u_{\mathrm{l},\lambda} = -\frac{gR^2}{\nu_{\mathrm{l}}^{\mathrm{m}}}\int_{\xi=1}^{\xi=\lambda}\beta(\xi)\,\mathrm{d}\xi \tag{46}$$

- To obtain the velocity of the liquid phase in the rest of the domain, integrate Eq. (44b) from $\xi = \lambda$ towards the column center using $u_{\mathrm{l},\lambda}$:

$$u_{\mathrm{l}} = u_{\mathrm{l},\lambda} - \frac{\nu_{\mathrm{l}}^{\mathrm{m}}R}{2l^2}\int_{\xi=\xi}^{\xi=\lambda}\left(1-\sqrt{1+\frac{4l^2gR}{\nu_{\mathrm{l}}^{\mathrm{m}^2}}\beta(\xi)}\right)\mathrm{d}\xi \tag{47}$$

- Substitute the so calculated radial profile of the axial liquid velocity into Eq. (45). If Eq. (45) is satisfied within the tolerance criterion, then the converged solution has been obtained. If the tolerance criterion is not met, then λ is incremented sequentially until convergence is achieved. A word of caution is in order at this point. The function defined by Eq. (44) could have steep gradients and proper care must be taken while integrating to obtain an accurate solution.

Once the liquid velocity profile and $\mathrm{d}p/\mathrm{d}z$ are determined as the converged solution to the one-dimensional liquid circulation model equations, we turn our attention back to the gas phase momentum equation. Combining Eqs. (23), (24) and (29), the expression for the slip velocity, u_{s}, is obtained.

$$u_{\mathrm{s}} = u_{\mathrm{g}} - u_{\mathrm{l}} = \sqrt{\frac{4d_{\mathrm{b}}(-\mathrm{d}p/\mathrm{d}z - \rho_{\mathrm{g}}g)}{3C_{\mathrm{D}}\rho_{\mathrm{l}}(1-\varepsilon_{\mathrm{g}})}} \tag{48}$$

Here, C_{D} is the drag coefficient and is a function of the slip velocity as well as of the bubble diameter and has to be obtained through an iterative scheme for a prescribed bubble diameter. Such an effective bubble diameter, representative of the entire domain, is obtained by iteratively searching for that bubble diameter which satisfies the overall gas phase continuity:

$$2\int_{\xi=0}^{\xi=1}\varepsilon_{\mathrm{g}}(\xi)u_{\mathrm{g}}(\xi)\xi\,\mathrm{d}\xi = \overbrace{2\int_{\xi=0}^{\xi=1}\varepsilon_{\mathrm{g}}(\xi)u_{\mathrm{l}}(\xi)\xi\,\mathrm{d}\xi}^{I_1} + \overbrace{2\int_{\xi=0}^{\xi=1}\varepsilon_{\mathrm{g}}(\xi)u_{\mathrm{s}}(\xi)\xi\,\mathrm{d}\xi}^{I_2} = U_{\mathrm{G,sup}} \tag{49}$$

The solution procedure for the gas phase velocity profile is based on adjusting the bubble diameter in the drag formulation via an iterative scheme to obtain a solution that satisfies gas phase continuity. The following steps are involved in this procedure.

- Guess a value for d_{b} (typically start with a very small value).
- Calculate $C_{\mathrm{D},1}$ as defined in Eq. (25). Since $C_{\mathrm{D},1}$ is independent of the radial coordinate ξ, as well as of the slip velocity u_{s}, once d_{b} is known, $C_{\mathrm{D},1}$ is simply evaluated based on the Eotvos number.
- Calculate $C_{\mathrm{D},2}$ as defined in Eq. (25). Since $C_{\mathrm{D},2}$ is a function both of ξ and u_{s}, it has to be evaluated at each ξ by the following Newton–Raphson procedure:

$$u_{\mathrm{s}}^{k+1} = u_{\mathrm{s}}^{k} - \frac{f(u_{\mathrm{s}}^{k})}{f'(u_{\mathrm{s}}^{k})} \tag{50}$$

$$f(u_{\mathrm{s}}) = u_{\mathrm{s}} - \sqrt{\frac{4d_{\mathrm{b}}(-\mathrm{d}p/\mathrm{d}z - \rho_{\mathrm{g}}g)}{3C_{\mathrm{D},2}\rho_{\mathrm{l}}(1-\varepsilon_{\mathrm{g}})}} \tag{51}$$

$$f'(u_{\mathrm{s}}) = \frac{\mathrm{d}f(u_{\mathrm{s}})}{\mathrm{d}u_{\mathrm{s}}} = 1 - \frac{24}{u_{\mathrm{s}}^2}\sqrt{\frac{\mu_{\mathrm{l}}^{\mathrm{m}^2}(-\mathrm{d}p/\mathrm{d}z - \rho_{\mathrm{g}}g)}{3\rho_{\mathrm{l}}^3C_{\mathrm{D},2}^3d_{\mathrm{b}}(1-\varepsilon_{\mathrm{g}})}} \tag{52}$$

- Calculate C_{D} as the maximum of $C_{\mathrm{D},1}$ and $C_{\mathrm{D},2}$ for each ξ, and subsequently calculate the radial profile of u_{s} from Eq. (48).
- Evaluate the gas phase mass balance using Eq. (49). The gas continuity is satisfied within the tolerance criterion, then the guessed bubble diameter is the correct one, otherwise d_{b} is incremented and the procedure is repeated until the tolerance criterion is met.

This solution procedure ensures that the overall gas phase mass balance is satisfied as part of the solution. Additionally, it provides an estimation of the bubble diameter, which is subsequently useful for calculating mass transfer coefficients. It should, however, be noted that the estimated bubble diameter depends on the drag formulation used, and therefore, it is important to use suitable drag correlation. In principle, any of the available drag forms could be used. This is an issue related to the sub-grid modeling of the phase interaction between the gas and liquid phases and is beyond the scope of this work. However, this is an important issue, as it is also relevant to the CFD simulations of flows in practical multi-phase systems. For the purposes of this study, we have adopted the formulation of Tomiyama et al. [39], as it is known to give reasonably good predictions over a wide range of bubble Reynolds numbers. It should also be mentioned that in its current form, the solution of the equations from the sub-model requires the knowledge of the radial gas holdup profile; therefore, the model is not fully predictive.

Before proceeding further, a precautionary note has also to be made about the converged liquid velocity profile. From Eq. (49), it can be seen that if the converged liquid velocity profile is such that the integral I_1 is greater than $U_{G,sup}$, it implies that an unphysical result has been obtained, since it would mean that in the long-time average sense, the gas phase is moving slower than the liquid, which obviously cannot be the case. The converged liquid velocity profile should therefore be checked for consistency after a converged solution satisfying liquid phase continuity has been achieved. If I_1 greater than $U_{G,sup}$ does indeed occur, it is indicative of gross inaccuracies in the gas holdup profile being used for solution of the model equations for liquid recirculation.

3.2. Parameter estimation

Once the radial profiles of the liquid/slurry and gas phase velocities are known, the various hydrodynamic input parameters for the mechanistic reactor model can be readily estimated. The liquid and gas velocity profiles obtained from the solution of the two-fluid recirculation model become zero at some radial locations. These are referred to as the inversion points with r' representing the inversion point for the liquid velocity, and r'' that for the gas. The inversion points are important in parameter estimation, as they define the boundaries of the four zones in the reactor model, viz., core and annulus flow regions for the gas and the liquid. The holdups of the gas and liquid/slurry in the various zones of the reactor are obtained from Eqs. (53)–(57) using the measured or estimated gas holdup profile.

Average liquid holdup in the up-flowing liquid region:

$$\bar{\varepsilon}_{l1} = \frac{2}{r'^2}\int_0^{r'} (1-\varepsilon_g) r \, dr \tag{53}$$

Average liquid holdup in the down-flowing liquid region:

$$\bar{\varepsilon}_{l2} = \frac{2}{R^2 - r'^2}\int_{r'}^{R} (1-\varepsilon_g) r \, dr \tag{54}$$

Average gas holdup in the up-flowing gas region:

$$\bar{\varepsilon}_{g1} = \frac{2}{r''^2}\int_0^{r''} \varepsilon_g r \, dr \tag{55}$$

Average gas holdup in the down-flowing gas region:

$$\bar{\varepsilon}_{g2} = \frac{2}{R^2 - r''^2}\int_{r''}^{R} \varepsilon_g r \, dr \tag{56}$$

Average gas holdup in the up-flowing gas and down-flowing liquid region:

$$\bar{\varepsilon}'_{g1} = \frac{2}{r''^2}\int_{r'}^{r''} \varepsilon_g r \, dr \tag{57}$$

From the converged solutions for the liquid and gas velocity profiles, the average velocities of the gas and liquid in the various zones are evaluated using Eqs. (58)–(61), and the mean slip velocity using Eq. (62). From Eqs. (49) and (62), an important observation to be made is that the actual mean slip velocity is always less than the apparent slip velocity, which is usually defined as $U_{G,sup}/\bar{\varepsilon}_g - U_{L,sup}/\bar{\varepsilon}_L$.

Average liquid velocity in the up-flowing liquid region

$$\bar{u}_{l1} = \frac{2\int_0^{r'} (1-\varepsilon_g)|u_l| r \, dr}{r'^2 \bar{\varepsilon}_{l1}} \tag{58}$$

Average liquid velocity in the down-flowing liquid region:

$$\bar{u}_{l2} = \frac{(2/\bar{\varepsilon}_{l2})\int_{r'}^{R} (1-\varepsilon_g) u_l r \, dr}{R^2 - r'^2} \tag{59}$$

Average gas velocity in the up-flowing gas region:

$$\bar{u}_{g1} = \frac{R^2 U_{G,sup} + 2\int_{r''}^{R} |u_g| \varepsilon_g r \, dr}{r''^2 \bar{\varepsilon}_{g1}} \quad (60)$$

Average gas velocity in the down-flowing gas region:

$$\bar{u}_{g2} = \frac{(2/\bar{\varepsilon}_{g2}) \int_{r''}^{R} |u_g| \varepsilon_g r \, dr}{R^2 - r''^2} \quad (61)$$

Average actual slip velocity:

$$U_{slip} = \frac{2\int_{\xi=0}^{\xi=1} \varepsilon_g(\xi) u_s(\xi) \xi \, d\xi}{\bar{\varepsilon}_g} \neq \frac{U_{G,sup}}{\bar{\varepsilon}_g} - \frac{U_{L,sup}}{\bar{\varepsilon}_l} \quad (62)$$

With the volumes and velocities associated with the various compartments of the reactor model estimated, the last set of parameters that need to be evaluated are the mass transfer coefficients and the interfacial areas for mass transfer. The volumetric mass transfer coefficient is widely studied and reported in the literature and numerous correlations are available for its estimation [7,42]. However, most of these correlations are empirical in nature with little fundamental basis and, therefore, usually work well only for systems similar to the ones from which data was obtained for their development. To incorporate some level of physics, in this study we have chosen to estimate the mass transfer coefficients based on the penetration theory by Higbie [43] and the interfacial areas have been evaluated using the bubble diameter that satisfies gas phase continuity. Following this methodology, one does not have to depend on empirical correlations for evaluating the mass transfer coefficients and interfacial areas as they can be readily calculated using Eqs. (63)–(70). These expressions assume the bubbles to be spherical, but one can apply suitable shape factor corrections if needed [44].

Interfacial area for mass transfer from up-flowing gas to up-flowing liquid:

$$a_{gulu} = \frac{6(\bar{\varepsilon}_{g1} - \bar{\varepsilon}'_{g1})}{d_b} \quad (63)$$

Interfacial area for mass transfer from up-flowing gas to down-flowing liquid:

$$a_{guld} = \frac{6\bar{\varepsilon}'_{g1}}{d_b} \quad (64)$$

Interfacial area for mass transfer from down-flowing gas to down-flowing liquid:

$$a_{gdld} = \frac{6\bar{\varepsilon}_{g2}}{d_b} \quad (65)$$

Interfacial area for mass transfer in distributor and disengagement CSTRs:

$$a_{CST} = \frac{6\bar{\varepsilon}_g}{d_b} \quad (66)$$

Mass transfer coefficient from up-flowing gas to up-flowing liquid:

$$k_{gulu} = \frac{2}{\sqrt{\pi}} \sqrt{\frac{D_{L,m}(\bar{u}_{g1} - \bar{u}_{l1})}{d_b}} \quad (67)$$

Mass transfer coefficient from up-flowing gas to down-flowing liquid:

$$k_{guld} = \frac{2}{\sqrt{\pi}} \sqrt{\frac{D_{L,m}(\bar{u}_{g1} + \bar{u}_{l2})}{d_b}} \quad (68)$$

Mass transfer coefficient from down-flowing gas to down-flowing liquid:

$$k_{gdld} = \frac{2}{\sqrt{\pi}} \sqrt{\frac{D_{L,m}(-\bar{u}_{g2} + \bar{u}_{l2})}{d_b}} \quad (69)$$

Mass transfer coefficient in distributor and disengagement CSTRs:

$$k_{CST} = \frac{2}{\sqrt{\pi}} \sqrt{\frac{D_{L,m} U_{slip}}{d_b}} \quad (70)$$

It should be noted that a constant bubble size has been used for estimating the "k_L" and "a" in the above equations which is rarely the case in a real system. We therefore investigated the effect of a bubble-size distribution on these parameters using a log-normal distribution. It was found that the volumetric mass transfer coefficient calculated based on average bubble size and an average slip velocity, estimated using this average bubble diameter, provided the upper bound for $k_L a$ as compared to $k_L a$ computed from the bubble-size and slip-velocity distributions. Moreover, as long as the normalized standard deviation for the chosen bubble-size distribution remained within 0.25 (for the two mean bubble sizes investigated, viz. 0.2 and 0.5 cm), this difference was within 10–15%.

Therefore, for the high pressure conditions encountered in industrial applications where the bubble sizes are generally in the range from 1–5 mm, the assumption of a constant bubble size for calculation of mass transfer effects is reasonable.

The above estimation procedure provides all the hydrodynamic model parameters needed to solve the reactor model equations. In Section 4, some results are presented both from simulation of the recirculation sub-model equations as well as from the reactor model mimicking gas tracer experiments in a pilot scale slurry bubble column under conditions of methanol synthesis.

4. Results and discussion

For solution of the model equations for gas and liquid recirculation, one needs to know two important inputs — the radial gas holdup profile and the closure for liquid/slurry phase turbulence. For the purposes of this study, the gas holdup profile is assumed to be known from experimental data, though some estimates for the average gas holdup could be obtained from correlations for systems where no experimental data exists [7,45,46]. In such cases, the value of the exponent m in Eq. (35) is usually assumed in the range of 2–5 [47] and c is assumed to be 1. On the other hand, the liquid phase turbulence in bubble column flows is usually assumed to be a superposition of the turbulence due to *shear* and that resulting from the highly oscillatory and dynamic bubble motion. The latter contributes to what is frequently referred to as the "bubble-induced" turbulence. Kumar et al. [22] investigated the existing literature on mixing length correlations relevant to bubble column flows and found that none of the existing forms matched all the data well. Therefore, based on their own experimental database as well as other data from the literature, they developed a mixing length form as represented by Eq. (40). This is empirical form but is known to provide reasonable estimates of the level of liquid circulation in the column. Another very simple form for mixing length (Eq. (42)) has been proposed by Joshi [41], which also performs reasonably well in predicting the levels of liquid recirculation. Additionally, there is the mixing length correlation of Nikuradse [40] developed for describing turbulent single-phase pipe flows. We first compare the performance of these three mixing length forms against two data sets for which measured liquid recirculation profiles are available from CARPT experiments.

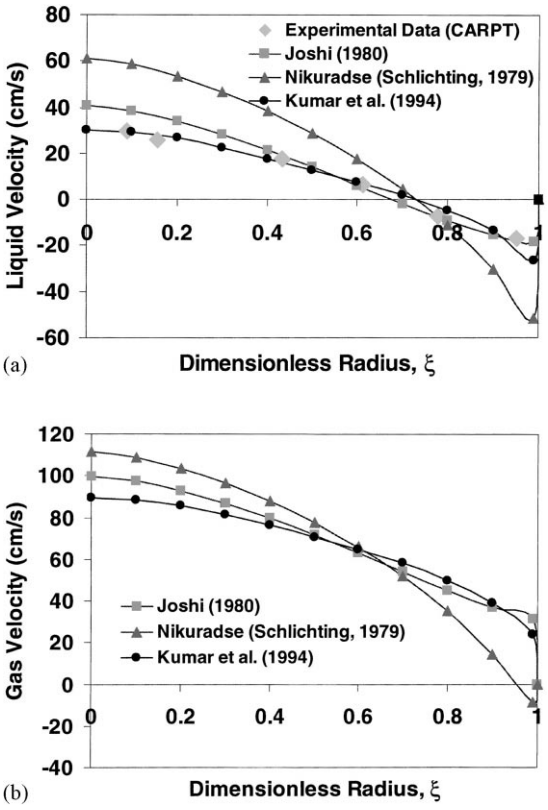

Fig. 3. Effect of mixing length profile on velocity profiles for 10 cm diameter bubble column operated at $U_{G,sup} = 12\,cm/s$: (a) liquid velocity; (b) gas velocity.

Figs. 3 and 4 show the relative performance of the three mixing length forms in predicting experimental data for the liquid phase recirculation. The experimental data is from two different columns, one of diameter 10 cm and the other one of diameter 44 cm. The superficial gas velocity for the former was maintained at $U_{G,sup} = 12\,cm/s$, while for the latter it was 10 cm/s. Nikuradse's mixing length always over-predicts the level of liquid recirculation since the effective turbulent viscosity from this formulation is only representative of the shear contribution to the total turbulence as in single-phase flows, and does not

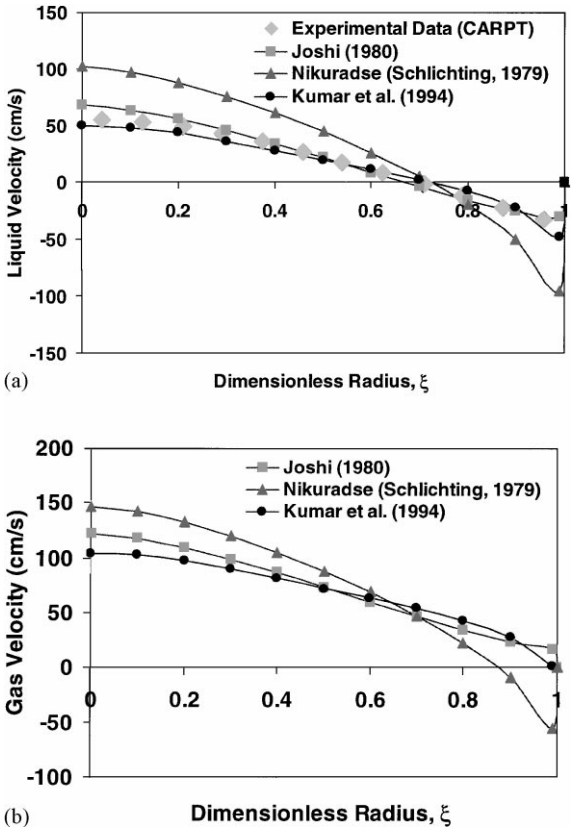

Fig. 4. Effect of mixing length profile on velocity profiles for a 44 cm diameter bubble column operated at $U_{G,sup} = 10$ cm/s: (a) liquid velocity; (b) gas velocity.

account for the increased turbulence generation and dissipation due to the presence of the bubbles. Therefore, for bubble column flows, use of Nikuradse's mixing length in solving for the liquid recirculation velocity profile is not recommended. Modifications to Nikuradse's mixing length could be sought to account for the bubble-induced turbulence, however, the dependence of mixing length on bubble diameter and its velocity fluctuation is not well established [23]. The correlations of Joshi [41] and Kumar et al. [22] give reasonable predictions for both the cases studied, though the correlation of Kumar et al. [22] seems to do somewhat better.

Next, we demonstrate the use of the gas–liquid recirculation sub-model to obtain the hydrodynamic input parameters to the mechanistic reactor model; subsequently, solve the bubble column model equations to predict radioactive gas tracer responses obtained in a 46 cm diameter pilot scale reactor undergoing liquid phase methanol synthesis. These experiments were conducted as part of the Department of Energy endeavor in developing slurry bubble column reactor technology for efficient conversion of synthesis gas (both from coal as well as natural gas) to alternate fuels and chemicals in the AFDU at La Porte, TX. The total dispersed phase height in the reactor was maintained at about 13.25 m from the distributor, and the reactor was operated at a pressure of 50 atm and a temperature of 250°C. The inlet superficial gas velocity was 25 cm/s. The gas superficial velocity decreased at the reactor exit due to a reduction in the total moles resulting from consumption of the synthesis gas and production of methanol. The average superficial gas velocity in the reactor was calculated as 22.86 cm/s.

Radioactive ^{41}Ar was injected at the bottom of the reactor into the gas inlet stream as the gas phase tracer. The evolution of its concentration inside the reactor was monitored at seven axial levels with the aid of scintillation counters. A sketch of the experimental setup for the tracer tests is shown in Fig. 5 with details presented elsewhere [21]. For comparison of the simulation results with experimental tracer responses, detector level 7 has been chosen in this study. Since the intensity counts measured by a scintillation counter are a complex function of the photon interaction with matter and the detector solid angle, it is not straightforward to relate the intensity counts to tracer concentration. Moreover, ^{41}Ar has a finite solubility in the slurry mixture and has its residence time prolonged by dissolving in the liquid. As a result, when comparing simulated results with experimental data, one has to include the contribution of the dissolved tracer in the slurry phase towards total scintillation counts registered by the counters. Therefore, the total tracer concentration at a given axial location needs to be calculated by summing the tracer concentrations in the gas and the liquid after appropriately weighting them by their respective holdups. Since the detectors are assumed to be reasonably shielded, it is justifiable to assume that at each detector level, the transient intensity counts when normalized by the maximum count would provide the correct basis for comparing experimental data against normalized

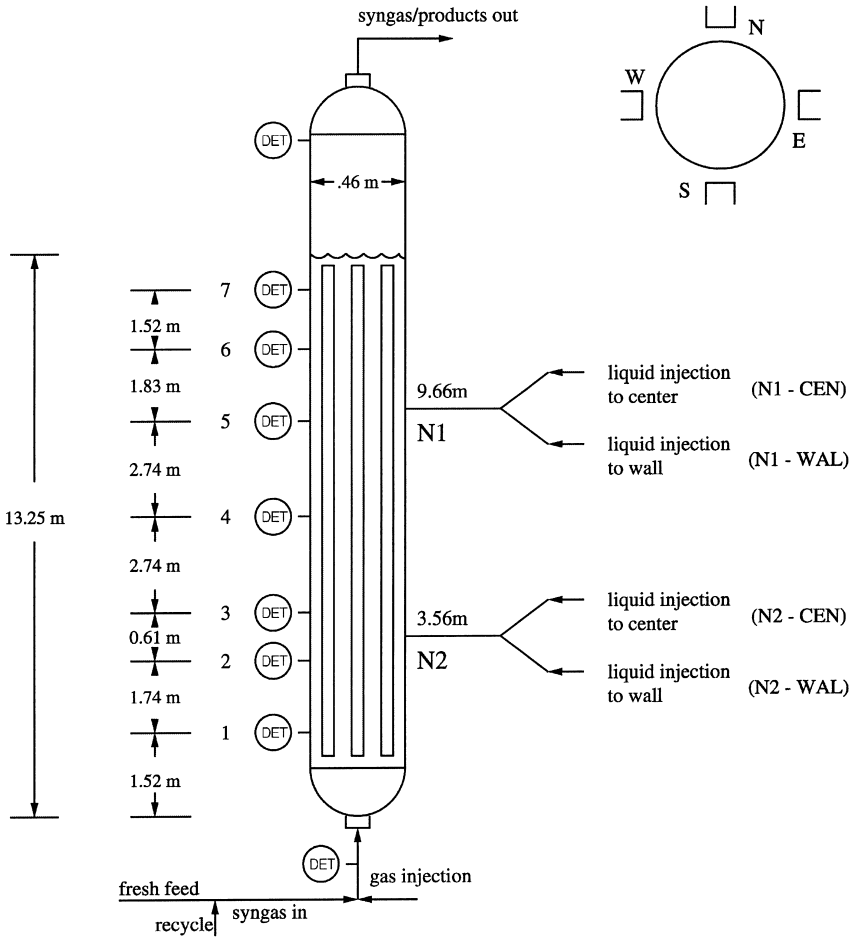

Fig. 5. Schematic representation of the pilot scale slurry bubble column at the AFDU, La Porte, TX indicating the detector levels for measurement of radioactive tracer responses [21].

total concentration at that axial plane. Fig. 6 shows the relative placement of the scintillation detectors with respect to the reactor insulation in one axial plane, as well as the various zones into which the reactor cross-section is compartmentalized. The normalized experimental tracer response curves shown in Figs. 7a and b are obtained by averaging the intensity counts registered by the four detectors at the axial plane corresponding to detector level 7. Since the gas as well as the entrained liquid move in a spiral motion as the gas rises up the column after its introduction at the sparger, radial mixing of the tracer is rapid. This mixing is reflected in the responses observed by the four individual detectors at a given location. Moreover, since the reactor model is not a three-dimensional representation of the transient distribution of any chemical species inside the reactor, modeling the process of detector-scintillation due to the tracer, by employing sophisticated and computationally involved Monte Carlo techniques [48], is not sought in the present study. In view of this, the best strategy is to compare the normalized total tracer response with the normalized average intensity counts registered at a given detector level. The total tracer concentration, which is subsequently normalized by its maximum for comparison with experimental data,

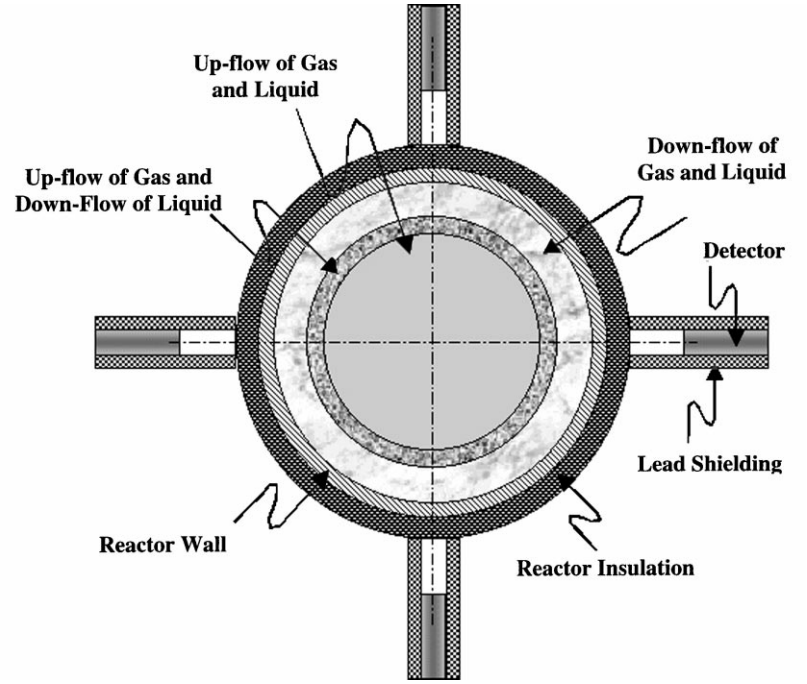

Fig. 6. Schematic representation of the AFDU reactor cross-section along with scintillation detectors and their lead shielding.

is given as

$$C_{\text{Total}} = C_{\text{g1}}(r''^2) + C_{\text{g2}}(1 - r''^2) + C_{\text{l1}}(r'^2) + C_{\text{l2}}(1 - r'^2) \quad (71)$$

Figs. 7a and b exhibit the comparison of the normalized experimental and simulation data, obtained from the mixing lengths of Joshi [41] and Kumar et al. [22], respectively, for several values of Henry's constant (representing the solubility of ^{41}Ar in the reactor slurry). The Henry's constant in this study is *dimensionless* and is defined as the ratio of the molar concentrations in the liquid and gas phases when the two phases are in equilibrium. The thermodynamically estimated value of the Henry's constant under the given operating conditions is about 0.17. This estimation procedure involves the assumption about the structure and mean molecular weight of the slurry mixture, and could deviate from the true value by ±25 to ±50%. Therefore, one needs to examine the effect of this parameter on the simulation results, which show high sensitivity to this parameter. The sensitivity to other parameters like the turbulent eddy diffusivities and volumes of the inlet and exit CSTRs is relatively insignificant as compared to the sensitivity with respect to Henry's constant.

From Figs. 7a and b, one can see that the parameters estimated using the mixing length profile of Kumar et al. [22] in general can provide a better agreement with the measured tracer response than those from the mixing length of Joshi [41]. Moreover, for a value of $H = 0.3$, and using the mixing length of Kumar et al. [22], one gets an excellent match of the simulated data with the experimental tracer response curve (Fig. 8). Such is not the case when using the mixing length of Joshi [41]. This is to be expected since the mixing length formulation of Kumar et al. [22], as mentioned earlier, provides better predictions of the liquid recirculation profiles, which subsequently gets reflected in the predictions obtained from the overall model equations. Altogether, this implies that a consistent prescription of the hydrodynamic inputs to the reactor model should result in reliable predictions, and provides fundamentally based criteria for design and

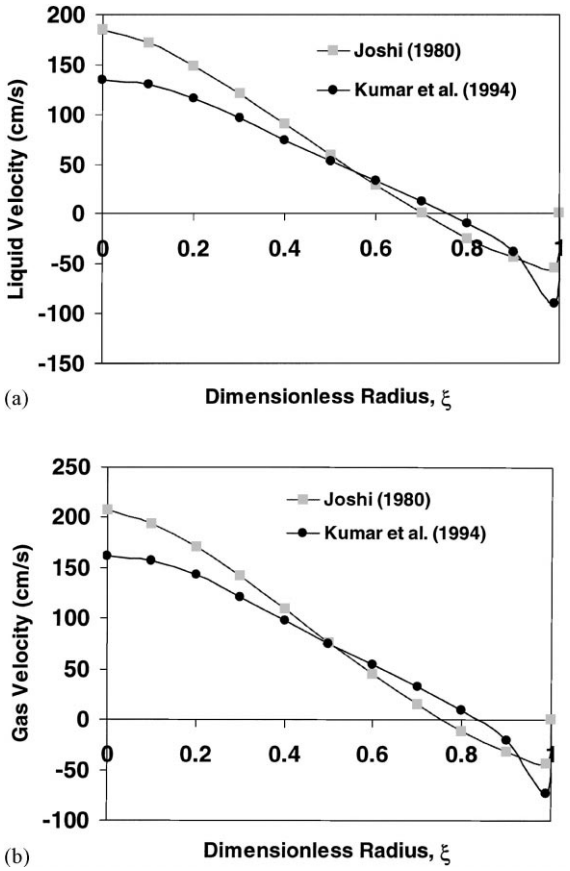

Fig. 7. Effect of mixing length profile on: (a) liquid and (b) gas velocity profiles for a 46 cm diameter pilot scale slurry bubble column operated at $U_{G,sup} = 22.86\,cm/s$.

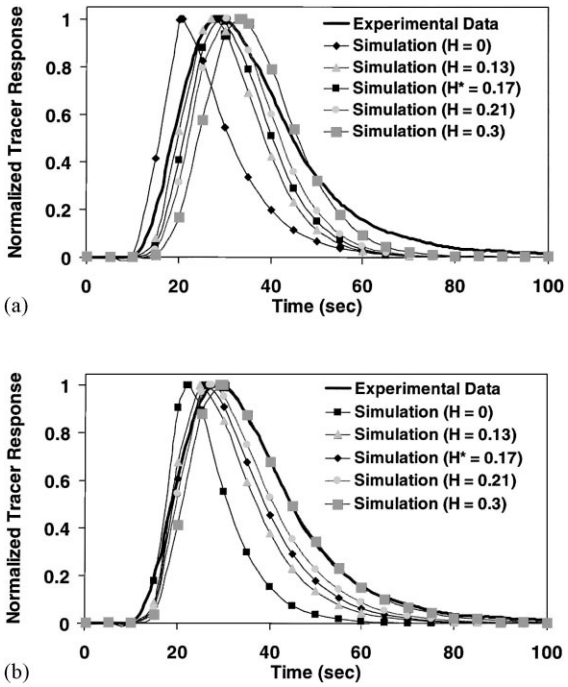

Fig. 8. Comparison of simulated and experimental radioactive gas tracer responses from a pilot scale slurry bubble column using mixing length formulations proposed by: (a) Joshi [41]; (b) Kumar et al. [22].

scale-up. It is also clear that mass transfer plays a significant role in governing the gas tracer distribution when one compares the simulation results for $H = 0$, and non-zero H with the experimental response.

5. Final remarks

In this study, a self-consistent hydrodynamic sub-model has been developed from the two-fluid equations describing two-phase flow in the Euler–Euler framework. The results from the solution of the model equations provide accurate predictions of the levels of liquid and gas recirculation when a proper closure for turbulence is used in the model equations. The hydrodynamic sub-model has been integrated into the four-zone mechanistic reactor model describing the distribution, generation and consumption of the reactant species. Comparison of the results from the mechanistic model with the experimental gas tracer data indicates good agreement between the two, provided a correct estimate for the solubility of the gaseous component in the liquid/slurry is available. The integrated predictive capabilities of the gas–liquid recirculation sub-model and the mechanistic reactor model do not suffer from the empiricism of the ADM, and therefore, provide a more reliable and fundamentally based methodology for design, synthesis, analysis and scale-up of bubble column reactors.

Acknowledgements

The authors gratefully acknowledge the continued support of this research from the Department of

Energy contract (DE-FC-22-95 PC 95051) through Air Products and Chemicals, Inc. and from the industrial sponsors of the Chemical Reaction Engineering Laboratory, Washington University.

References

[1] I. Wender, Fuel Process. Technol. 48 (1996) 189.
[2] S.T. Sie, R. Krishna, Appl. Catal. A 186 (1999) 55.
[3] R.A. Mashelkar, Br. Chem. Eng. 15 (1970) 1297.
[4] Y.T. Shah, ACS Symp. Ser. (Chem. React.) 168 (1981) 203.
[5] W.-D. Deckwer, ACS Symp. Ser. (Chem. React.) 168 (1981) 213.
[6] M.A. Kohler, Appl. Catal. 22 (1986) 21.
[7] F. Kastanek, J. Zahradnik, J. Kratochvil, J. Cermak, Chemical Reactions for Gas–Liquid Systems, Ellis Horwood, New York, 1993, p. 244 (Chapter 4).
[8] J.B. Joshi, U. Parasu Veera, Ch.V. Prasad, D.V. Phanikumar, N.S. Deshphande, S.S. Thakre, B.N. Thorat, PINSA-A, Proceedings of the Indian National Science Academics, Part A, Vol. 64, 1998, p. 441.
[9] M. Lopez de Bertodano, R.T. Lahey Jr., O.C. Jones, Int. J. Multiphase Flow 20 (1994) 805.
[10] F. Larachi, J. Chaouki, G. Kennedy, M.P. Dudukovic, in: J. Chaouki, F. Larachi, M.P. Dudukovic (Eds.), Non-Invasive Monitoring of Multiphase Flows, Elsevier, New York, 1997, p. 335 (Chapter 11).
[11] D.A. Drew, S.L. Passman, Theory of Multicomponent Fluids, Springer, New York, 1998, p. 121 (Chapter 11).
[12] J.A.M. Kuipers, W.P.M. Van Swaaij, Adv. Chem. Eng. 24 (1998) 227.
[13] R. Krishna, M.I. Urseanu, J.M. van Baten, J. Ellenberger, Chem. Eng. Sci. 54 (1999) 4903.
[14] M.P. Dudukovic, Catal. Today 48 (1999) 5.
[15] M.P. Dudukovic, AIChE Symp. Ser. (Adv. Technol. Fluid-Particle Syst.) 321 (1999) 30.
[16] Y. Pan, M.P. Dudukovic, M. Chang, Chem. Eng. Sci. 54 (1999) 2481.
[17] A. Sokolichin, G. Eigenberger, Chem. Eng. Sci. 54 (1999) 2273.
[18] S.S. Thakre, J.B. Joshi, Chem. Eng. Sci. 54 (1999) 5055.
[19] K.J. Myers, M.P. Dudukovic, P.A. Ramachandran, Chem. Eng. Sci. 42 (1986) 2301.
[20] S. Degaleesan, S. Roy, S.B. Kumar, M.P. Dudukovic, Chem. Eng. Sci. 51 (1996) 1967.
[21] S. Degaleesan, Fluid dynamic measurements and modeling of liquid mixing in bubble columns, D.Sc. Thesis, Washington University, St. Louis, MO, 1997.
[22] S.B. Kumar, N. Devanathan, D. Moslemian, M.P. Dudukovic, Chem. Eng. Sci. 49 (1994) 5637.
[23] N.W. Geary, R.G. Rice, AIChE J. 38 (1992) 76.
[24] H. Luo, H.F. Svendsen, Can. J. Chem. Eng. 69 (1991) 1389.
[25] R.G. Rice, N.W. Geary, AIChE J. 36 (1990) 1339.
[26] K. Ueyama, T. Miyauchi, AIChE J. 25 (1979) 258.
[27] R. Nottenkamper, A. Steiff, P.-M. Weinspach, Ger. Chem. Eng. 6 (1983) 147.
[28] T. Menzel, T. in der Weide, O. Staudacher, O. Wein, U. Onken, Ind. Eng. Chem. Res. 29 (1990) 988.
[29] B.P. Yao, C. Zheng, H.E. Gasche, H. Hofmann, Chem. Eng. Process. 29 (1991) 25.
[30] R.F. Mudde, J.S. Groen, H.E.A. Van Den Akker, Chem. Eng. Sci. 52 (1997) 4217.
[31] R.F. Mudde, J.S. Groen, H.E.A. Van Den Akker, Nucl. Eng. Des. 184 (1998) 329.
[32] N. Devanathan, D. Moslemian, M.P. Dudukovic, Chem. Eng. Sci. 45 (1990) 2285.
[33] N. Devanathan, Investigation of liquid hydrodynamics in bubble columns via a computer automated radioactive particle tracking (CARPT), D.Sc. Thesis, Washington University, St. Louis, MO, 1991.
[34] S.B. Kumar, D. Moslemian, M.P. Dudukovic, Flow Meas. Instr. 6 (1995) 61.
[35] S.B. Kumar, D. Moslemian, M.P. Dudukovic, AIChE J. 43 (1997) 1414.
[36] J. Chen, P. Gupta, S. Degaleesan, M.H. Al-Dahhan, M.P. Dudukovic, B.A. Toseland, Flow Meas. Instr. 9 (1998) 91.
[37] Q. Wang, Modeling of gas and liquid phase mixing with reaction in bubble column reactors, M.S. Thesis, Washington University, St. Louis, MO, 1996.
[38] P. Gupta, M.H. Al-Dahhan, M.P. Dudukovic, B.A. Toseland, Chem. Eng. Sci. (2000), in press (for presentation at ISCRE-16, Poland).
[39] A. Tomiyama, I. Kataoka, T. Sakaguchi, Trans. JSME, Part B 61 (1995) 2357.
[40] H. Schlichting, Boundary Layer Theory, McGraw-Hill, New York, 1979, p. 510 (Chapter 20).
[41] J.B. Joshi, Trans. Inst. Chem. Engrs. 58 (1980) 155.
[42] D. Azbel, Two-Phase Flows in Chemical Engineering, Cambridge University Press, Cambridge, 1981, p. 157 (Chapter 7).
[43] P.V. Danckwerts, Gas–Liquid Reactions, McGraw-Hill, New York, 1970, p. 96 (Chapter 5).
[44] R. Clift, J.R. Grace, M.E. Weber, Bubbles, Drops, and Particles, Academic Press, New York, 1978, p. 169 (Chapter 7).
[45] X. Luo, D.J. Lee, R. Lau, G. Yang, L.S. Fan, AIChE J. 42 (1999) 665.
[46] A. Kemoun, B.C. Ong, P. Gupta, M.H. Al-Dahhan, M.P. Dudukovic, Int. J. Multiphase Flows (2000), in press.
[47] S.D. Gharat, J.B. Joshi, Chem. Eng. J., Biochem. Eng. J. 48 (1992) 141.
[48] N. Tsoulfanidis, Measurement and Detection of Radiation, McGraw-Hill, New York, 1983, p. 247 (Chapter 8).